SCIENTIFIC OASIS

Decision Making: Applications in Management and Engineering

Journal homepage: www.dmame-journal.org
ISSN: 2560-6018, eISSN: 2620-0104

Application of an Optimized Version of Modified Elman Neural Network Using Improved Pelican Optimizer for Energy System Marginal Price Forecasting

Yuanchun Tang[1], Shichun Chen[2], Zhuolin Chen[3,*] Ying Shi[4]

1 State Grid Fujian Electric Power Research Institute, Fuzhou, Fujian, China. Email: chenyishuan786894@163.com
2 State Grid Fujian Electric Power Co., Ltd., Fuzhou, Fujian, China. Email: zhangjunch558110@163.com
3 State Grid Fujian Electric Power Research Institute, Fuzhou, Fujian, China. Email: chenzhuolin2026@163.com
4 State Grid Fujian Electric Power Research Institute, Fuzhou, Fujian, China. Email: bcrlzik87622883@163.com

ARTICLE INFO

Article history:
Received 5 April 2025
Received in revised form 19 May 2025
Accepted 7 June 2025
Available online 29 December 2025

Keywords:
System Marginal Price, Prediction, Modified Elman Neural Network, Fréchet distance, Improved Pelican Optimization Algorithm.

ABSTRACT

Following the liberalisation of the electricity sector and its transition to a competitive market structure, price volatility has intensified, as electricity tariffs are now formed through market-based pricing mechanisms. Electricity price time series exhibit complex properties, including pronounced instability, strong non-linearity, and substantial fluctuations. In response to these characteristics, this study concentrates on the development of a day-ahead system marginal price (SMP) forecasting framework based on an enhanced Elman Neural Network (ENN). To improve the predictive capability of the proposed ENN, a modified pelican optimisation algorithm is employed to optimise its parameters. For the selection of short-term input variables, the Pearson correlation coefficient is applied to identify the most relevant factors. In contrast, long-term input variables are determined by incorporating the discrete Fréchet distance, alongside seasonal attributes, day-type information, forecasted load, and historical SMP values. A comprehensive dataset spanning fifteen years is used to evaluate the effectiveness of the proposed model. The empirical results demonstrate that the suggested approach achieves superior forecasting accuracy compared with conventional SMP prediction methods, confirming its effectiveness for electricity market price forecasting.

1. Introduction

The gradual transition from monopolistic electricity markets to competitive market structures, together with the transfer of public-sector responsibilities to private entities, has progressively altered the economic behaviour of firms operating within the electricity sector, despite enduring structural differences across systems [1]. This transformation has introduced new operational conditions and risk exposures for market participants, as competitive electricity markets increasingly resemble other traded commodity markets [2; 5; 7]. Within this environment, firms pursue strategies aimed at maximising revenue while simultaneously limiting costs and mitigating

* *Corresponding author.*
E-mail address: chenzhuolin2026@163.com

https://doi.org/10.31081/dmame8220251606

exposure to uncertainty. A central objective for suppliers operating in restructured electricity markets is the effective management of financial risk, which primarily arises from price volatility and fluctuations in demand volume [10].

Over the past decade, extensive regulatory reforms have substantially reshaped the organisation and operation of electricity networks. These reforms have dismantled the traditional vertically integrated structure of energy utilities, leading to a fundamental reconfiguration of their operational and managerial frameworks. In jurisdictions where such reforms have been implemented, electricity generation, transmission, and distribution activities have been fully unbundled and assigned to separate entities. Unlike previous arrangements, in which a single authority managed all operational stages, each component of the restructured electricity system now functions independently according to its own objectives and operational characteristics [11; 13; 14; 17; 18]. Although these components remain technically interconnected, their economic activities are governed by market mechanisms rather than central coordination, necessitating the establishment of organised markets to align economic incentives.

The intensification of competition within electricity markets has made accurate electricity price forecasting indispensable for all market participants. Precise price predictions enable utilities to design effective supply strategies, optimise bilateral contractual arrangements, and reduce exposure to financial risk [3]. At the same time, consumers depend on reliable cost forecasts to guide consumption decisions and identify opportunities to minimise electricity-related expenditures. As competitive electricity markets have evolved, the structural importance of price indicators such as SMP has increased considerably [22; 24]. SMP constitutes a critical informational signal for electricity producers and energy-related firms seeking to improve profitability in competitive environments [6]. However, forecasting SMP remains particularly challenging, as electricity is widely recognised as one of the most volatile commodities traded in modern markets.

SMP may vary rapidly, often on an hourly basis, in response to the continuous balancing of electricity supply and demand. In addition, SMP is influenced by multiple external factors, including fuel price dynamics, infrastructure development, and long-term contractual agreements between suppliers and consumers. Consequently, the development of a robust and adaptable SMP forecasting framework capable of capturing both short-term and long-term price dynamics is essential. Within the organisation and management of the energy sector, SMP forecasting represents a comprehensive and strategically significant process [25; 27; 34]. Over the past two decades, numerous forecasting approaches have been proposed, reflecting diverse economic perspectives and technical methodologies. In parallel, accurate load forecasting has become a fundamental task in the planning of electricity distribution networks, as it supports investment decision-making and facilitates efficient project scheduling [36].

Efficient operation of the electricity sector depends on meeting multiple performance criteria, including system reliability and operational security [33]. The inherently volatile nature of electricity demand requires operators to allocate sufficient generation and transmission capacity to ensure supply stability, while aligning technical planning with financial evaluation to control operating costs. The foundation of such analyses lies in forecasting accuracy, as errors directly affect the financial performance of grid management and system control activities [8]. During operational stages, heightened uncertainty or conservative system utilisation further amplifies sensitivity to forecasting inaccuracies [9; 15]. Forecasting errors may result in inefficient operational decisions, such as unnecessary energy purchases, suboptimal electricity sales, or the avoidance of unit shutdowns associated with high start-up costs, all of which impose additional financial burdens [20; 32]. Historically, electricity price forecasting relied primarily on statistical analysis techniques; however, these approaches have shown limitations in capturing the complex dynamics of restructured electricity markets.

In recent years, a wide range of advanced techniques has been introduced to improve SMP forecasting performance. Among these, neural network-based methods have demonstrated strong potential for reducing prediction errors and enhancing operational efficiency. Load forecasting remains one of the most critical tasks in the operation and maintenance of electricity systems, as improved accuracy directly supports more effective system planning. Neural network techniques have gained increasing attention as predictive tools due to their strong capabilities in classification, functional approximation, and complex pattern mapping [37]. A key advantage of these models lies in their ability to learn intricate pricing behaviours that are difficult or computationally intensive to identify using conventional analytical approaches [38].

Several studies have examined the application of advanced modelling techniques to SMP forecasting. One study developed a day-ahead SMP prediction framework using artificial neural networks combined with similarity-based information, demonstrating improved accuracy through the application of k-fold cross-validation and long-term historical data [28]. Using fifteen years of historical load and SMP data, the proposed method outperformed traditional forecasting approaches. Another investigation applied nonlinear autoregressive exogenous models and multilayer perceptron's to SMP forecasting within the Korean electricity market, comparing results with those obtained using Autoregressive Integrated Moving Average models across multiple forecasting horizons [28]. The findings indicated that all approaches achieved relatively low forecasting errors, with optimal performance dependent on model configuration and hidden node selection.

Additional research evaluated machine learning techniques for day-ahead SMP forecasting within the Italian electricity market [40]. Key explanatory variables included lagged SMP values and cross-market price indicators. Results showed that training models on larger datasets improved predictive accuracy, while sensitivity analysis revealed that modest data perturbations could substantially increase forecasting error metrics. Long-term SMP forecasting has also been addressed using error correction models that incorporate fuel price information [31]. These approaches demonstrated strong out-of-sample performance, particularly when accounting for long-run equilibrium relationships between SMP and natural gas prices. Furthermore, the operation of Smart Microgrids under carbon taxation and environmental policy constraints has been investigated, showing that systems integrating Distributed Energy Resources (DER) and Renewable Energy Sources (RES) can simultaneously reduce CO2 emissions and operational costs while maintaining reliable performance, assuming grid connectivity and accounting for emissions from imported electricity [4].

Building on these findings, the present research proposes a day-ahead SMP forecasting framework that integrates both short-term and long-term statistical information. Long-term historical data are incorporated to enhance predictive accuracy, leading to the classification of input parameters into short-term type input variables (STIV) and long-term type input variables (LTIV). STIV are selected using Pearson correlation analysis, while LTIV incorporate a season and day indicator (SDI) derived from discrete Fréchet distance analysis, which captures hourly SMP pattern similarities across different day types. By combining recent and historical information, the proposed framework constructs a comprehensive input set for SMP prediction. The final forecasting model is developed through the integration of a modified ENN with an enhanced pelican optimisation algorithm, which has demonstrated strong capability in identifying complex patterns when handling a large number of input parameters.

2. System Definition

SMP is determined by the interaction between electricity demand and generation costs. Consequently, it reflects the balance between economic dispatch decisions and the anticipated level of electricity demand. Electricity generation is scheduled to satisfy forecasted demand at the

minimum possible cost, and SMP is calculated based on the highest marginal generation cost among the dispatched power units [16; 19]. Under this mechanism, energy service providers prioritise generation bids with the lowest production costs, and dispatch continues incrementally in ascending order of generation cost until the forecasted demand is fully satisfied. The dominant component of generation cost is associated with the procurement of primary energy resources. Accordingly, SMP is strongly influenced by the cost of acquiring these energy inputs, which exhibits considerable temporal variability [35]. This study examines the evolution of SMP behaviour and develops a forecasting framework using historical data collected in South Korea over the period from 2001 to 2016. The analysed data reveal a dynamic pattern characterised by increasing electricity demand and persistent fluctuations in primary energy prices over time. These long-term variations indicate that short-term forecasting approaches alone are insufficient for accurate day-ahead SMP prediction, as they fail to capture underlying long-term price movements. Therefore, to effectively extract the latent information embedded within historical SMP patterns, it is essential to analyse both long-term and short-term data simultaneously.

2.1. Analysis of Short-Term Historical SMP Data

Short-term historical data consist of information associated with the prediction time and encompass hourly observations extending back to the previous week. These data are categorised into two groups, namely hourly-based variables and daily-based variables, both defined at each hour of analysis. Hourly-based data include observations from the hour immediately preceding the forecasted time and extend backward over the previous twenty-three hours, for example from Py,d,t1 to Py,d,t23. In contrast, daily-based data incorporate observations recorded at the same hour of the forecasted time for each of the preceding seven days, for example from Py,d1,t to Py,d7,t. To determine the most relevant candidates for short-term input variables, the Pearson correlation coefficient (PCC) is employed as the selection criterion. PCC is utilised to quantify the strength of the linear relationship between potential input variables and the target output, thereby enabling the identification of variables with the highest predictive relevance. The technical formulation of PCC is presented as follows.

$$V_{icc}^{m} = \frac{n \times (\sum X^{m} Y) - (\sum X^{m}) \times (\sum Y)}{\sqrt{\left(n \times (\sum (X^{m})^{2}) - (\sum (X^{m})^{2})\right) \times \left(n \times (\sum Y^{2}) - (\sum Y^{2})\right)}} \quad (1)$$

Where, n describes data number, V_{icc}^{m} stands for the input variable number m's correlation coefficient, X^{m} describes the input variable number m, and Y signifies the output. Fig. (1) illustrates the results obtained from the Pearson Correlation Coefficient analysis conducted on both an hourly and daily basis.

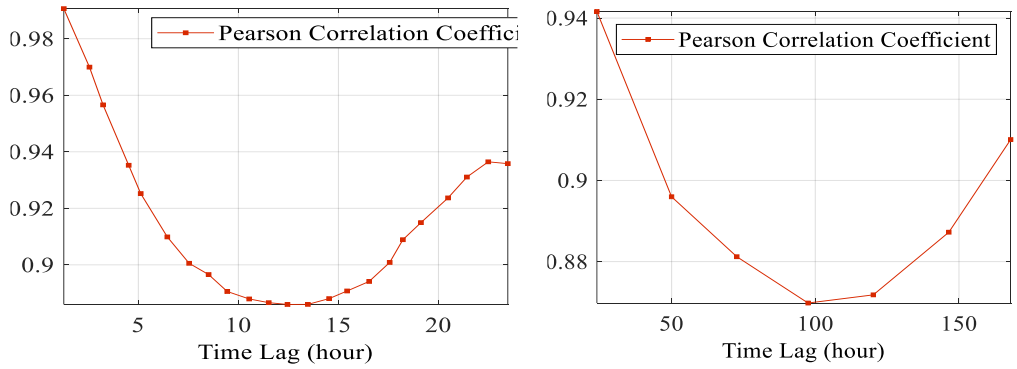

(A) (B)

Fig. 1: Findings of Pearson Correlation Coefficient at Every Hour and Every Day Basis (A) Up to the Preceding 24 h, and (B) Up to the Preceding Week

Based on the assessed significance of the correlation coefficients, the final selection of STIV is conducted from the set of candidate input variables. The statistical relevance of each correlation coefficient is examined through the application of a t-test, which is used to evaluate the corresponding null hypothesis regarding the significance of the observed correlation. As a result, the STIVs provide the previous hour's short-term type input variables ($P_{y,d,t-1}$), the same hour of the previous day ($P_{y,d-1,t}$), and the identical hour of the prior week ($P_{y,d-7,t}$). The forecasted load also exerts a notable influence on SMP. The Pearson correlation coefficient was calculated for the year 2016 using one year of historical data, resulting in a value of 0.53, which indicates a moderately positive relationship between the predicted load and SMP. As a result, the predicted load ($L_{y,d,t}$) is added as an input variable. As a result, the predicted load's historical data at the same time as the historical system marginal price are included and designated as $L_{y,d,t-1}$, $L_{y,d-1,t}$, and $L_{y,d-7,t}$ that define the predicted load at the preceding time, the predicting load at the same time on previous day, and predicted load at the same time in preceding week.

2.2. Analysis of Long-Term Historical SMP Data

Data collected over the same periods in previous years are regarded as long-term historical data. To assemble an extended dataset for SMP, fifteen years of records, spanning from 1 January 2001 to 31 December 2016, were analysed. This historical information serves two primary purposes. The first purpose is to incorporate the long-term fluctuation patterns of SMP when constructing forecasting models. Fig. (2) depicts the variations in SMP trends over the fifteen-year period.

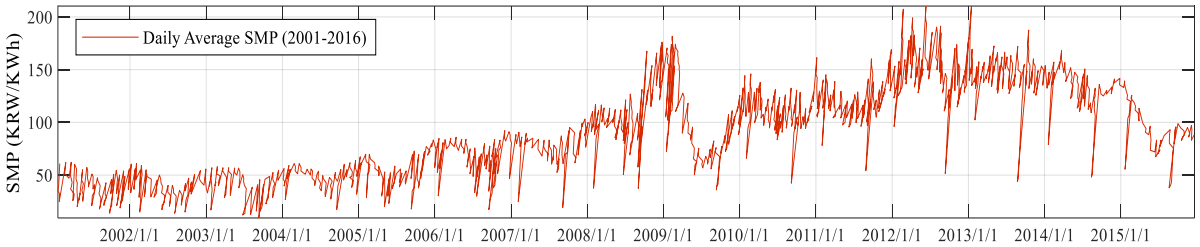

Fig. 2: The Trend Varies Over a Period of 15 Years in Korea

As illustrated in Fig. (2), the daily average SMP in Korea exhibits temporal variation driven by changes in electricity demand and fluctuations in the cost of primary energy procurement. During the initial five years, SMP values remain relatively low and stable. Beginning in 2006, a linear increase is observed, followed by a sharp decline in 2009, after which SMP rises rapidly again in 2010. The values remain steady until 2012, with a slight upward trend towards the end of that year, and subsequently show a general tendency to decrease. Consequently, when constructing forecasting models, long-term historical data are regarded as capturing the underlying developmental trends of SMP. The second purpose of analysing long-term historical data is to extract specific SMP patterns for selected days. Examination of fifteen years of historical records reveals that certain days exhibit distinctive behaviour. Fig. (3) presents the days in 2016 that display anomalous SMP patterns compared with typical days.

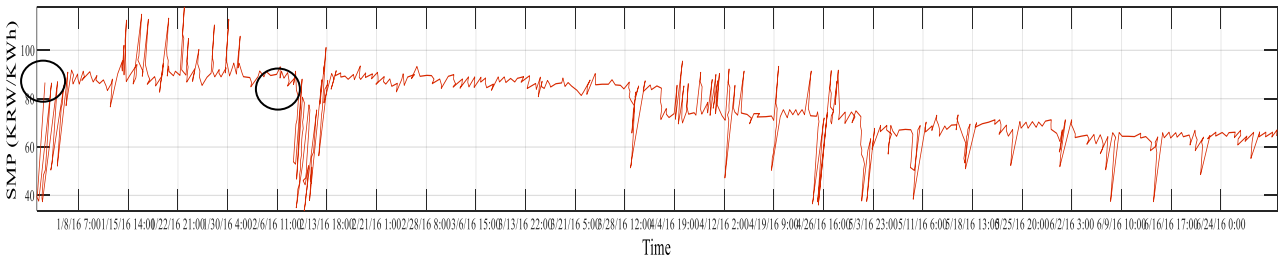

Fig. 3: SMP Hourly Pattern from January 1 to June 30, 2016

The days exhibiting distinctive SMP patterns are indicated by black circles. The limited availability of data for such atypical days presents challenges in constructing accurate forecasting models, which may reduce predictive performance. Therefore, incorporating long-term historical data provides additional insights into these uncommon patterns. Accordingly, both SMP and forecasted load from previous years are included as components of the LTIV corresponding to the same forecasted time. $P_{y-1,d,t}$, $L_{y-1,d,t}$, $P_{y-2,d,t}$, $L_{y-2,d,t}$, …, $P_{y-15,d,t}$, $L_{y-15,d,t}$ are the variables' notational units.

3. Fréchet Distance

In some cases, historical data from earlier years within the long-term dataset may not exhibit patterns comparable to the forecasted day, which can reduce the accuracy of predictions. To address this, only historical days that demonstrate similarity to the forecasted day are utilised as input variables in the proposed method, effectively serving as reference days. Following the methodology in [28], the Fréchet distance is employed to quantify the similarity between days. This measure evaluates the degree of similarity between two curves by considering both the shapes of the curves and the spatial positions of points along them. Unlike the conventional Euclidean norm, the Fréchet distance provides a more suitable metric for comparing SMP patterns across different days. It is determined how much the separate Fréchet distance between curves P and curves Q ($D_{df}^{P,Q}$) is as follows [12]:

$$D_{df}^{P,Q} = \min(\max d(\dot{p}_i, \dot{q}_k)) \tag{2}$$

$$d(p,q) = \|p - q\| = \sqrt{\sum_j (p_j - q_j)^2} \tag{3}$$

Where, $\dot{p}_j$ and $\dot{q}_k$ represent, in turn, the j^{th} and k^{th} discrete points of curves P and Q that may be obtained via the Fourier transformation. $d(p,q)$ signifies the symbols represents the separation between p and q, which have the coordinates p_j and q_j.

The calculated discrete Fréchet distances are categorised into four groups, yielding four principal hourly SMP patterns. These patterns are subsequently utilised in the development of a dedicated forecasting model. Furthermore, the identified patterns are generalised into a set of reference criteria to compute the Fréchet distance for the forecasted day. The generalisation procedure takes into account historical Fréchet distances, seasonal effects, and day-type characteristics, including holidays and working days. The following section outlines the essential assumptions underlying the Fréchet distance calculation:

Holiday in Spring Season

$$D_{df} \in [0.2,0.3] \tag{4}$$

Holiday in Other Season

$$D_{df} \in [0.3, 0.4] \tag{5}$$

Lunar New Year and Thanksgiving Day

$$D_{df} \in [0,0.1] \tag{6}$$

In Other Days

$$D_{df} > 0.4 \tag{7}$$

The challenge of discrepancies between the forecast day and reference days can be addressed through the application of the Fréchet distance. Each day is assigned a Fréchet distance value, and the selection of reference SMP data from historical records is adjusted according to the Fréchet distance of the forecasted day. If the Fréchet distance of a candidate reference day differs from that of the predicted day, the reference is shifted to an earlier or later day until alignment is achieved

[39]. This adjustment process continues iteratively until the Fréchet distance of the reference day matches that of the forecast day.

The algorithm finds the nearby earlier or next day that has an Fréchet distance comparable to that of the forecast day, for instance, if it's supposed that there is a difference between the Fréchet distance of the forecast day and the Fréchet distance of the historical data (for instance, $D_{df}(y-1,d,t)=2$ and $D_{df}(y,d,t)=1$). So, the modified long-term type input variable are $P^{a}_{y-1,d,t}, P^{a}_{y-2,d,t}, \dots, P^{a}_{y-15,d,t}$. The equivalent predicted load for the considered points is defined as $L^{a}_{y-1,d,t}, L^{a}_{y-2,d,t}, \dots, L^{a}_{y-15,d,t}$. The pseudocode outlining the steps of this methodology is presented as follows:

Algorithm 1: Pseudocode of the Fréchet Distance Tuning for Choosing Input Parameters
Start Choose STIPs (short-term input parameters), including: $P_{y,d,t-1}, P_{y,d-1,t}, P_{y,d-7,t}, L_{y,d,t}, L_{y,d,t-1}, L_{y,d-1,t}, L_{y,d-7,t}$ Choose LTIPs (long-term input parameters), including: $P_{y-1,d,t}, \dots\dots, P_{y-15,d,t}, L_{y-1,d,t}, \dots\dots, L_{y-15,d,t}$ IF, SDI of LTIP is equal to SDI of predict Day: Choose Updated LTIP, including: $P^{U}{}_{y-1,d,t}, \dots\dots, P^{U}{}_{y-15,d,t}, L^{U}{}_{y-1,d,t}, \dots\dots, L^{U}{}_{y-15,d,t}$ Else: Discover the nearest SDI-based LTIP: ($P^{U}{}_{y-i,d,t} = P_{y-i,d\mp1,t}, L^{U}{}_{y-i,d,t} = L_{y-i,d\mp1,t}$) End if Train the data END

4. Elman Neural Networks

In this section, SMP forecasting is conducted using the ENN. The advent of artificial neural networks has introduced a novel paradigm in applied science and engineering, enabling solutions to problems that were previously difficult to address using conventional methods. Tasks such as pattern recognition, data clustering, time series forecasting, electricity price prediction, satellite navigation, routing, and robotic control, which traditionally posed significant analytical challenges, can now be approached with increased accuracy and efficiency through neural network methodologies. Artificial neural networks are parallel information-processing systems inspired by the structure and function of biological neural networks. The primary objective in developing such systems is to construct a mathematical model that emulates human learning and reasoning through network architectures capable of rapid information processing. Neural networks consist of numerous fundamental processing units, referred to as neurons, which are interconnected via synaptic links associated with adjustable weight parameters. These adaptive weights encode the knowledge acquired by the network, which is essential for performing specific tasks. Neural networks have been widely applied across engineering domains, including electricity price forecasting. The Elman network is a type of multi-layer neural network. While Markov models provide a robust analytical framework, the ENN incorporates principles inspired by Markov processes, representing this concept within a hidden layer. The network architecture comprises four primary layers: the input layer, context layer, hidden layer, and output layer. Fig. (4) presents a simplified schematic of the ENN structure.

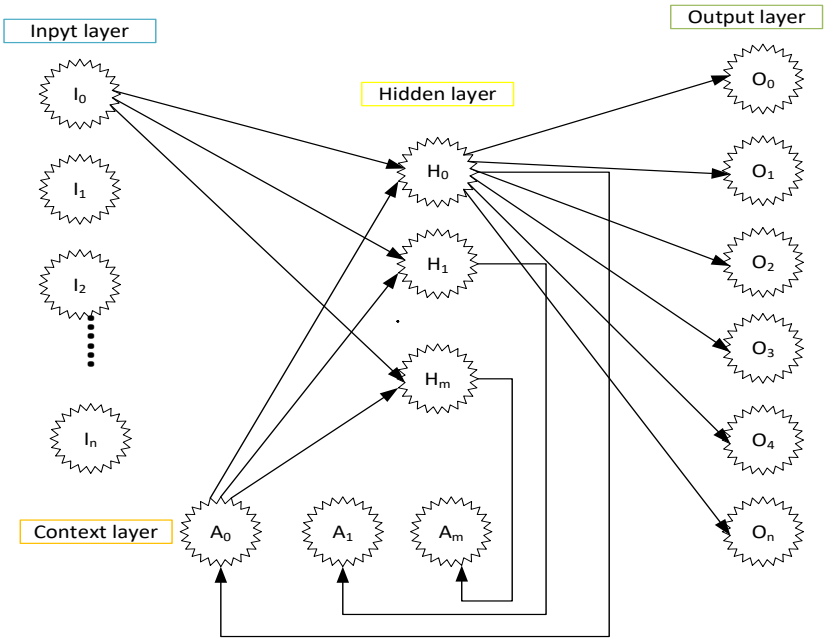

Fig. 4. Simple Arrangement of the Elman Neural Network

The ENN illustrated in Fig. (4) consists of a single hidden layer. Outputs from the hidden-layer neurons are fed back into the network through time-delayed units, known as context units, which functionally act as additional input nodes for the network. The network's output is therefore a non-linear transformation that depends both on the current external inputs and on the hidden-layer activations from the preceding timestep. Recurrent connections between the hidden layer and context units possess fixed weight coefficients, allowing the network to process temporal information and capture dependencies across observed sequences. As a result, training the ENN is generally less complex than training a conventional feedforward network with standard error backpropagation. While it shares many operational similarities with traditional backpropagation networks, the ENN benefits from the one-step-ahead feedback mechanism, which accelerates the learning process. Mathematically, the input layer of the ENN is expressed as follows:

$$I_i(l) = e_i(l), \quad (8)$$

Where, l defines the iteration number, and $i = 1,2,\ldots,n$.

Subsequently, the output of the hidden layer, denoted as layer k, in the ENN is represented by the following equation:

$$v_k(l) = \sum_{j=1}^{N} \omega_{kj}^{1}(l) x_j^c(l) + \sum_{i=1}^{n} \omega_{ki}^{2}(l) u_i(l) \quad (9)$$

$$k = 1,2,\ldots,N$$

Where, $x_j^c(l)$ labels the transmitted data from the contextual node k, $\omega_{kj}^{1}(l)$ designates number j and number j weights for the hidden layers.

Consequently, for the input layer (I), the hidden layer (k) weight has been attained by $\omega_{ki}^{2}(l)$. Consequently, the integration of the hidden layer output into the context layer is performed according to the following procedure:

$$W_k(l) = f_o(\bar{v}_k(l)) \quad (10)$$

Where,

$$\bar{v}_k(l) = \frac{v_k(l)}{max[v_k(l)]} \quad (11)$$

represents the normalised value of the hidden layer output.

The context layer is mathematically defined as follows:

$$C_k(l) = \beta C_k(l-1) + W_k(l-1), \quad (12)$$
$$k = 1,2,\ldots,N$$

Where, W_k signifies the self-connected feedback gain in the range [0, 1] [36].

Finally, the output of the network is computed using the following equation:

$$y_o(l) = \sum_{k=1}^{N} \omega_{ok}^3(l) W_k(l), \quad (13)$$
$$o = 1,2,\ldots,n$$

Where, ω_{ok}^3 represent the connection weight by the layer k into layer O.

W_h^i, W_h^c, and W_h^o describe the weight of input matrix, context matrix, and output matrix, respectively. The input and output layers dimension are n, that is:

$$\begin{bmatrix} x^1(t) \\ y(t) \end{bmatrix} = \begin{bmatrix} x_1^1(t), x_2^1(t), \ldots, x_n^1(t) \\ y_1(t), y_2(t), \ldots, y_n(t) \end{bmatrix}^T \quad (14)$$

Although, the context layer dimension is m.

A novel approach proposed in [38] was employed to modify the ENN, enhancing both learning accuracy and convergence, as illustrated in Fig. (5).

Initializing the learning rate value $\mu = \varepsilon$
In the l^{th} iteration:
if $l \leq 2$:
$\mu = defaultvalue;$
end if $t >= 3$ && $1.02e(l-1) > e(l)$:

$$\mu = c\frac{(1+\frac{1}{l})^l}{exp(1)}$$

else
$\mu = defaultvalue$
end
end
Weights updating;
evaluate $e(t)$;
if the stop criteria are reached:
break;
else
continue

Fig. 5: Improved Elman Neural Network

Where, t signifies the present epoch, c describes a constant, and μ stands for the learning rate. In this research, the weights of the modified ENN are optimised using an enhanced variant of the Pelican Optimization Algorithm.

5. Improved Pelican Optimization Algorithm

The population-based Pelican Optimization Algorithm and its associated mathematical formulation are initially introduced.

5.1. Motivation and Pelican Behaviour throughout Hunting

Pelicans possess a large pouch in their pharynx, which they use to capture and ingest their prey. These birds are highly social and typically form groups that can number in the hundreds. While turtles, frogs, and crustaceans are occasionally consumed, fish constitute the primary component of

their diet. Pelicans generally hunt cooperatively, coordinating their movements to improve efficiency. During hunting, a pelican identifies its target and dives from a considerable height, typically between 10 and 20 metres. Certain pelican variants, however, approach their prey from lower altitudes. Upon reaching the water, they extend their wings parallel to the surface, creating a disturbance that drives fish into shallower areas, thereby facilitating capture. Before swallowing their prey, pelicans tilt their heads downward to expel excess water ingested during the hunt. The structured hunting strategies of pelicans demonstrate their proficiency as predators. These behavioural mechanisms inspired the development of the proposed algorithm, which incorporates analogous strategies to enhance optimisation performance.

5.2. The Suggested POA Mathematical Model

Within this computational model, each pelican agent represents a candidate solution within the population of the algorithm. The optimisation variables are defined according to their spatial positions within the solution space. The population is initially generated using stochastic methods while adhering to predetermined boundary conditions, including upper and lower limits.

$$z_{i,j} = l_j + rand.\left(u_j - l_j\right), i = 1,2,\dots,N, \quad j = 1,2,\dots,m, \tag{15}$$

Where, $z_{i,j}$ indicates the significance of the j^{th} variable determined by the i^{th} individual solution, N represents the number of population candidate, m indicates the numeral of problem variables, $rand$ defines a random amount between 0 and 1, l_j and u_j describe the j^{th} lower and upper bound of decision variables.

In the proposed POA, the population matrix presented below characterises the members of the pelican population. Each row of the matrix corresponds to an individual solution, while the columns represent the respective values of the decision variables for the optimisation problem.

$$Z = \begin{bmatrix} Z_1 \\ \vdots \\ Z_i \\ \vdots \\ Z_N \end{bmatrix}_{N\times m} = \begin{bmatrix} z_{1,1} & \cdots & z_{1,j} & \cdots & z_{1,m} \\ \vdots & \ddots & \vdots & \iddots & \iddots \\ z_{i,1} & \cdots & z_{i,j} & \cdots & z_{i,m} \\ \vdots & \iddots & \vdots & \ddots & \vdots \\ z_{N,1} & \cdots & z_{N,j} & \cdots & z_{N,m} \end{bmatrix}_{N\times m} \tag{16}$$

Where Z and Z_i represent the pelicans population matrix and the i^{th} pelican.

Based on the individual solutions defined above, the fitness function for the given problem can be evaluated. The resulting fitness function vector, presented below, indicates the computed fitness values for each solution.

$$F = \begin{bmatrix} F_1 \\ \vdots \\ F_i \\ \vdots \\ F_N \end{bmatrix}_{N\times 1} = \begin{bmatrix} F(Z_1) \\ \vdots \\ F(Z_i) \\ \vdots \\ F(Z_N) \end{bmatrix}_{N\times 1} \tag{17}$$

Where the fitness function amount of the i^{th} individual solution is denoted by F_i.

The individual solution vectors are iteratively updated by mimicking the offensive and prey-capturing behaviours of pelicans. The algorithm's simulation consists of two principal stages: exploration, which models movement toward the prey, and exploitation, which replicates winging actions along the water surface to maximise capture efficiency.

Step 1: Exploration (Movement in the Direction of the Prey)

Once the hunting location is established by the pelican, it moves toward this target. In the

algorithm, this movement simulates the search within the solution space and represents the exploration capability of the POA in identifying diverse regions within that space. It is important to note that in the POA, the hunting locations are generated randomly within the solution domain, which enhances the algorithm's exploratory performance during the search for optimal solutions. The mathematical formulation corresponding to the process described above is as follows:

$$z_{i,j}^{P_1} = \begin{cases} z_{i,j} + rand.\left(p_j - I.z_{i,j}\right), & F_p < F_i \\ z_{i,j} + rand.\left(z_{i,j} - p_j\right), & else \end{cases} \quad (18)$$

Where $z_{i,j}^{P_1}$ denotes the novel place of the i^{th} pelican in the j^{th} dimension according to this step, I is a random value the same as 2 or 1, which is chosen in any iteration and for any individual, p_j represents the place of prey in the j^{th} dimension, and F_p indicates its cost function amount. When the parameter I is set to two, it induces greater movement of a population member, enabling the search of previously unexplored regions of the solution space. The precision of the solution space analysis is influenced by the chosen value of I. Updates to the pelican's position are accepted only if they lead to an improvement in the fitness function, ensuring that the algorithm avoids non-optimal regions. The corresponding governing equations for this procedure are formulated as follows:

$$Z_i = \begin{cases} Z_i^{P_1}, F_i^{P_1} < F_i; \\ Z_i, \ else, \end{cases} \quad (19)$$

Where $Z_i^{P_1}$ defines the novel situation of the i^{th} pelican and $F_i^{P_1}$ indicates its fitness function value on the basis of step 1.

Step 2: Exploitation (Winging on the Plane of the Water)

When the pelican descends to the water surface and extends its wings, the fish are driven upward and captured. By simulating this hunting behaviour, pelicans can seize a large number of fish efficiently. In the context of the POA, this mechanism enables convergence toward superior solutions within the search space, thereby enhancing the algorithm's local search capability and exploitation efficiency. From a mathematical perspective, achieving convergence toward an optimal solution requires a structured evaluation of the neighbourhood surrounding the pelican's position. This behaviour is represented by the following equation:

$$z_{i,j}^{P_2} = z_{i,j} + R.\left(1 - \frac{t}{T}\right).(2.rand - 1).z_{i,j}, \quad (20)$$

Where $z_{i,j}^{P_2}$ defines the novel situation of the i^{th} pelican in the j^{th} dimension according to this step, R is a constant value the same as 0.2, $R.\left(1 - \frac{t}{T}\right)$ indicates the neighborhood radius of $z_{i,j}$, t is the iteration numerator, T represents the max number of iteration. The ability to exploitation of POA in order to approach the universally convergent solution is influenced by the hyperparameter " $R.\left(1 - \frac{t}{T}\right)$". The magnitude of this coefficient diminishes as the algorithm progresses, resulting in a gradual reduction of the neighbourhood radius. In essence, this coefficient enables a finer-resolution examination of the local topology surrounding each candidate solution. Consequently, the POA is able to converge toward solutions that are closer to the global, or even the absolute global, optimum.

The following equation formalises the update mechanism used to accept or reject a pelican's new position:

$$Z_i = \begin{cases} Z_i^{P_2}, F_i^{P_2} < F_i; \\ Z_i, \ else, \end{cases} \quad (21)$$

Where $Z_i^{P_2}$ represents the novel situation of the i^{th} pelican and $F_i^{P_2}$ indicates its fitness function

value on the basis of step 2.

Repetition of Steps, Pseudo-Code: Once all individual members have been updated following the procedures outlined above, the elite solution is iteratively refined by considering both the newly generated positions of the population members and their associated fitness values. The algorithmic steps are then repeated according to the governing equations described previously. Ultimately, the best solution obtained over the course of the iterations is presented as a quasi-optimal solution to the given problem. The corresponding POA pseudo-code is provided below.

Algorithm 2: Pseudocode of POA
Start POA. Enter the information of the optimization problem. Specify the POA individuals size (N) and the numeral of iteration. Initialization of the location of pelicans and compute the fitness function. For $t = 1: T$. Create the location of the prey randomly. For $I = 1: N$. Step 1: exploration (movement in the direction of the prey). For $j = 1: m$. Compute novel situation of the j^{th} dimension utilizing Eq. (4). End. Renew the i^{th} individuals member utilizing Eq. (5). Step 2: exploitation (winging on the plane of the water). For $j = 1: m$. Compute novel situation of the j^{th} dimension utilizing Eq. (6). End. Renew the i^{th} individuals member utilizing Eq. (7). End. Renew finest individual solution. End. Output finest solution achieved by POA. End POA.

5.3. Improved Pelican Optimization Algorithm (IPOA)

Certain limitations of the conventional Pelican Optimization Algorithm, including the random replacement of the least fit pelicans and insufficient exploitation, can result in slow convergence. The original POA has been critically examined, and various enhancements have been proposed to address these shortcomings. In this study, two specific modifications are introduced to improve the efficiency of the POA in overcoming these issues [29]. The first modification incorporates the Lévy flight mechanism. Lévy flight, widely adopted in optimisation algorithms, is founded on principles of stochastic movement and is modelled using random walk theory. The Lévy flight ($\boldsymbol{F_l}$) should be formulated by the following equation:

$$F_l(\alpha) \cong 1/\beta^{1+\tau} \quad (22)$$

$$\alpha = A/|B|^{1/\tau},\ A, B \sim N(0, \sigma^2) \quad (23)$$

$$\sigma^2 = \left\{\frac{\sin(\pi\tau/2)}{2^{(1+\tau)/2}} \times \frac{\Gamma(1+\tau)}{\tau\Gamma((1+\tau)/2)}\right\}^{\frac{2}{\tau}} \quad (24)$$

Where, τ signifies the constant of the Lévy flight and is set 1.5 Li et al. [23], β represents the size of step, and $\Gamma(.)$ defines the Gamma function.

Accordingly, the steps of the enhanced mechanism can be expressed using the following equation:

$$z_{i,j}^{P_1} = \begin{cases} z_{i,j} + F_l(\sigma).\left(p_j - I.z_{i,j}\right), & F_p < F_i \\ z_{i,j} + F_l(\sigma).\left(z_{i,j} - p_j\right), & else \end{cases} \quad (25)$$

The second enhancement involves incorporating a chaos mechanism into the algorithm. The chaos mechanism is typically represented by the following formulation:

$$CM_{i+1}^{j} = f\left(CM_i^j\right) \quad (26)$$

$$j = 1,2,\ldots,N$$

Where, $f\left(CM_i^j\right)$ defines generator function, N signifies the map [30].

By analysing various chaotic functions, this study selected the sinusoidal chaotic map as a representative chaos mechanism. This method employs pseudo-random numbers rather than purely random ones, enhancing the algorithm's initial convergence and lowering computational complexity. Consequently, the motion of the population members is adjusted according to this modification. Under the revised formulation, the generation of population individuals is determined as follows:

$$z_{i+1,j}^{new} = \left(z_{i,j}\right)^2 \sin\left(\pi z_{i,j}\right) \quad (27)$$

Where, $z_{0,j} = rand(.)$.

Algorithm Authorization

The performance of the proposed improved Pelican Optimization Algorithm must be evaluated using a set of widely recognised benchmark functions to demonstrate its effectiveness. To this end, the enhanced POA is applied to several standard test functions, including Levi No. 03, Six-hump Camel, Leon, and Schwefel functions, in order to validate its optimisation capability. The mathematical definitions of these functions are as follows:

Six-Hump Camel: This benchmark function features six local minima, of which two correspond to the global optima. The parameter space is restricted by x_1 = [-3, 3] and x_2 = [-2, 2]. The function is analysed using the following relation:

$$f_1(z) = \left(4 - 2.1z_1^2 + \frac{z_1^4}{3}\right)z_1^2 + z_1 \times z_2 + (-4 + 4z_2^2) \times z_2^2 \quad (28)$$

Levi No. 03: This benchmark function is highly non-convex. The Levi No. 03 function, defined over a two-dimensional solution space, represents a multimodal optimisation problem. The domain for all variables is limited to the interval [-10, 10]. The corresponding objective function for Levi No. 03 is expressed using the following equation:

$$f_2(z) = \sin^2(3\pi z_1) + (z_1 - 1)^2\left(1 + \sin^2(3\pi z_2)\right) + (z_2 - 1)^2\left(1 + \sin^2(2\pi z_2)\right) \quad (29)$$

Schweffel: The Schwefel function is a challenging benchmark characterised by multiple local minima. Its search domain is typically represented as an n-dimensional hypercube, with each variable ranging from -500 to 500, defined as follows:

$$f_3(z) = 418.9829d - \sum_{i=1}^{d} z_i \, sin\left(\sqrt{|z_i|}\right) \quad (30)$$

The Leon Function: This benchmark function is continuous, non-convex, and defined over a two-dimensional solution space. The Leon function is recognised as relatively complex and has been extensively used in optimisation studies. It is defined over the interval [0, 10], and its fitness value is calculated using the following equation:

$$f_4(z) = 100(z_2 - z_1^3)^2 + (1 - z_1)^2 \quad (31)$$

The results produced by the proposed method are subsequently validated through comparison with two established optimisation techniques: the Multi-Verse Optimizer (MVO) [42] and the Owl Search Algorithm (OSA) [43]. Table 1 presents the parameter settings employed for these optimisation algorithms.

Table 1
Set Parameters of the Optimization Algorithms

Algorithm	Parameter	Value
Multi-Verse Optimizer (MVO) Mirjalili et al. [26]	WEP_{min}	0.2
	WEP_{max}	1
	$Coefficient\ (P)$	6
Owl Search Algorithm (OSA) Jain et al. [21]	T_{dead}	18
	$\|P\|$	10
	Acc_{low}	0.2
	Acc_{high}	1

For all algorithms, the population size and the maximum number of iterations were set to 50 and 200, respectively, to ensure reliability and comparability of the results. The simulations were conducted on a system with 8.0 GB of memory, an Intel Core i7 CPU at 2.00 GHz, and a 64-bit operating system. The performance of the proposed improved Pelican Optimization Algorithm, compared with other optimizers, is presented in Table 2, based on evaluation metrics including minimum, maximum, mean, and standard deviation (SD) values. Table 2 indicates that the enhanced Pelican Optimization Algorithm (POA) surpasses other comparable optimisation methods in terms of solution accuracy for the selected benchmark functions, successfully identifying optimal solutions even with a limited population size. The algorithm's robustness is further demonstrated by its consistently lower SD values compared with alternative approaches. These findings validate the effectiveness of the proposed method in tackling complex optimisation problems. In this study, the improved POA is applied to achieve optimal energy management and component sizing within hybrid systems.

Table 2
Review of the Suggested Optimization Method's Objective Function Analysis

Algorithm	Index	F1	F2	F3	F4
MVO Mirjalili et al. [26]	Min	17.5968e-8	9.1183	7.8831	5.4857e-4
	Max	15.6728e-3	19.2731	11.8992	6.6567e-2
	AVG	22.6527-6	14.8263	9.8665	7.4755e-3
	SD	13.5488-6	12.5591	7.2387	6.3364e-3
OSA Jain et al. [21]	Min	15.1587e-13	7.5884	3.8437e-3	4.5683-5
	Max	26.6784-9	16.4894	4.5361e-1	6.2154e-3
	AVG	21.0864-11	11.7572	3.7351-2	5.5938e-4
	SD	20.5922-11	12.4435	2.8495e-2	4.1882e-4
IPOA	Min	11.5491e-18	5.5878	4.4740-5	5.1688-6
	Max	19.6687-14	11.2886	3.2788	8.0735e-4
	AVG	16.4782-16	9.8237	2.8457	7.8848e-5
	SD	15.6766-16	8.5262	3.4351e-3	6.1941e-5

6. Results and Discussion

The simulation environment for this study was implemented using MATLAB version 2017b on a notebook equipped with an AMD A4 3600 CPU, 8 GB of RAM, and a 64-bit Windows 10 operating system. For all algorithms, the number of iterations and population size were set to 200 and 40, respectively. To ensure reliability, each approach was executed independently 30 times. The

simulation, following the methodology described in the preceding sections, was conducted to predict the day-ahead SMP for 2017. The accuracy of the proposed model was evaluated against a standard Artificial Neural Network (ANN) employed as a reference model. The performance of the SMP forecasting model was assessed using the Mean Absolute Percentage Error (MAPE), which measures the effectiveness by computing the percentage difference between the predicted and actual SMP values. Mathematically, MAPE is expressed as follows:

$$f_{MAPE}(\%) = \frac{1}{N}\left(\sum_{j=1}^{N} \frac{P_j^{observed} - P_j^{predict}}{P_j^{observed}}\right) \times 100 \tag{32}$$

Table 3 presents the overall average MAPE of the proposed model in predicting the SMP for 2017. Additionally, the table provides the average MAPE values for all Fréchet distances (FD) throughout 2017. As shown in Table 3, the proposed model (ANN incorporating Fréchet distance) achieves a more accurate forecast, with a total average MAPE of 3.91%, compared to 5.45% for the conventional ANN-based model. The proposed approach also demonstrates enhanced performance in predicting days characterised by different Fréchet distances. For further validation, the improved method (ENN/IPOA) is compared against the modified ENN without optimization (ENN). The simulation results are analysed in detail using temporal SMP curves, where representative daily profiles are selected according to the Fréchet distance classification criteria.

Table 3
The Overall Mean Absolute Percentage Error Average of the Model is used to Predict the System Marginal Price in 2017

	Entire Mean MAPE	Mean MAPE FD=1	Mean MAPE FD =2	Mean MAPE FD =3	Mean MAPE FD =4
Conventional ENN	5.45%	26.36%	6.61%	6.94%	4.31%
ENN/IPOA	3.91%	17.55%	5.12%	5.56%	2.87%
Total Days	365	8	32	83	246

6.1. Day Prediction When Fréchet Distance is 1

The Fréchet distance for Korea's major holidays, specifically Lunar New Year and Thanksgiving Day, is equal to 1. In 2017, these holidays fell on October 4–6 for Thanksgiving Day and January 27–30 for Lunar New Year. The predicted SMP for January 28, 2017, is illustrated in Fig. (6). For days with a Fréchet distance of 1, the proposed ENN/IPOA model achieves a daily MAPE of 13.65%, whereas the conventional ENN model records a daily MAPE of 16.44%. This comparison demonstrates that the suggested model provides more accurate SMP predictions than the standard ENN on these significant holiday periods.

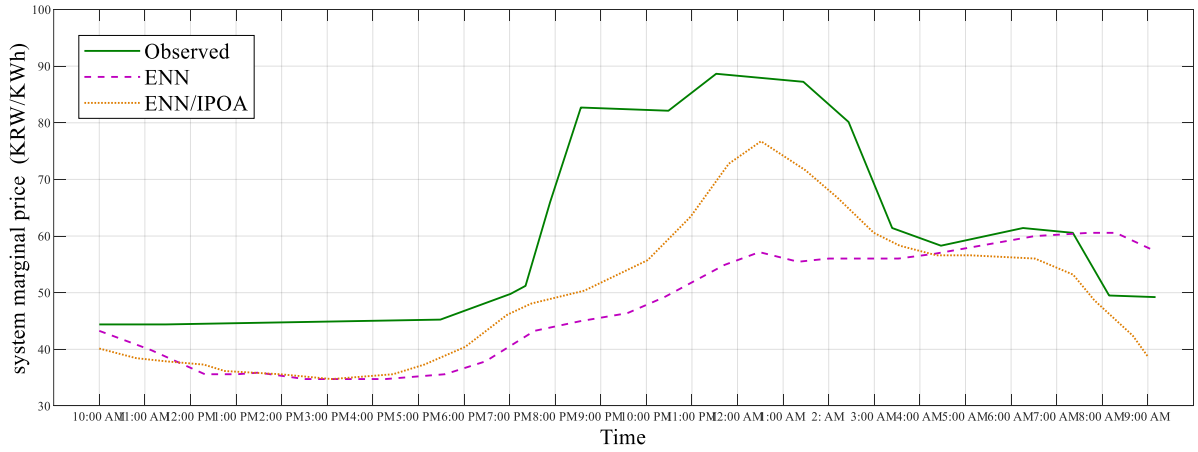

Fig. 6: Outcome of the System Marginal Price Predicting on January 28

6.2. Day Prediction When Fréchet Distance is 2

Certain holidays and seasonal events, including Labour Day (May 1), Independence Movement Day (March 1), Children's Day (May 5), and Buddha's Birthday (observed May 3), are assigned a FD of 2 in the analysis. Figure 7 illustrates the predicted SMP profile for March 1 as a representative example. As shown in Fig. (7), the conventional ENN model achieves a MAPE of 8.16%, whereas the proposed ENN/IPOA model attains a significantly lower MAPE of 1.96%, demonstrating superior accuracy in SMP prediction.

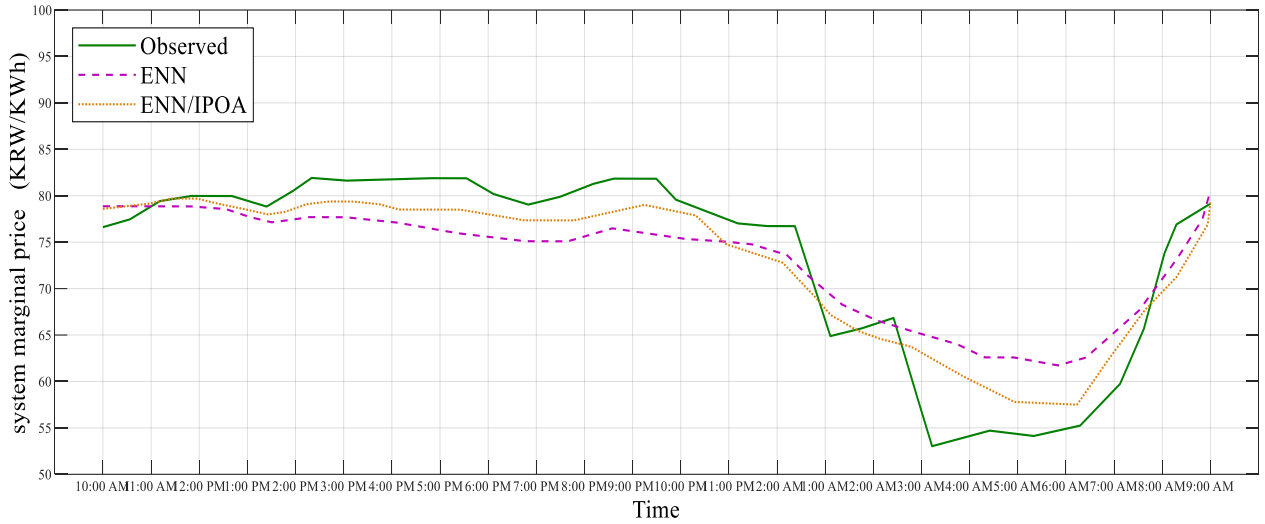

Fig. 7: Outcome of the System Marginal Price Predicting for March 1

6.3. Day Prediction When Fréchet Distance is 3

Days with a Fréchet distance (FD) of 3 include holidays and Sundays occurring outside of the spring season, excluding Lunar New Year and Thanksgiving Day. This FD category encompasses August 15 (Liberation Day), December 25 (Christmas Day), and January 1 (New Year's Day). Figure 8 presents the predicted SMP outcomes for August 15. The conventional ENN model forecasts SMP with a MAPE of 6.16%, while the proposed ENN/IPOA model achieves a lower MAPE of 3.86%, indicating improved prediction accuracy.

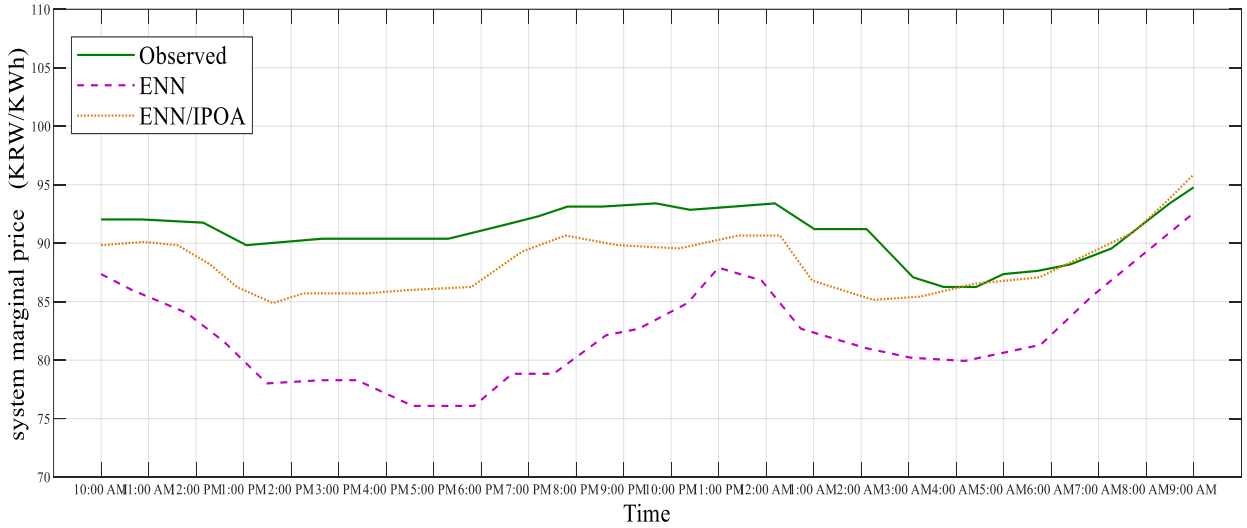

Fig. 8: Outcomes of the System Marginal Price Prediction for August 15

6.4. Day Prediction When Fréchet Distance is 4

Days not classified under the previous FD categories are considered to have a FD of 4. Figure 9

illustrates the predicted SMP for January 19, which serves as a representative example of typical days. The conventional ENN model predicts SMP with a MAPE of 2.46%, whereas the proposed ENN/IPOA model attains a lower MAPE of 1.28%, demonstrating enhanced forecasting precision.

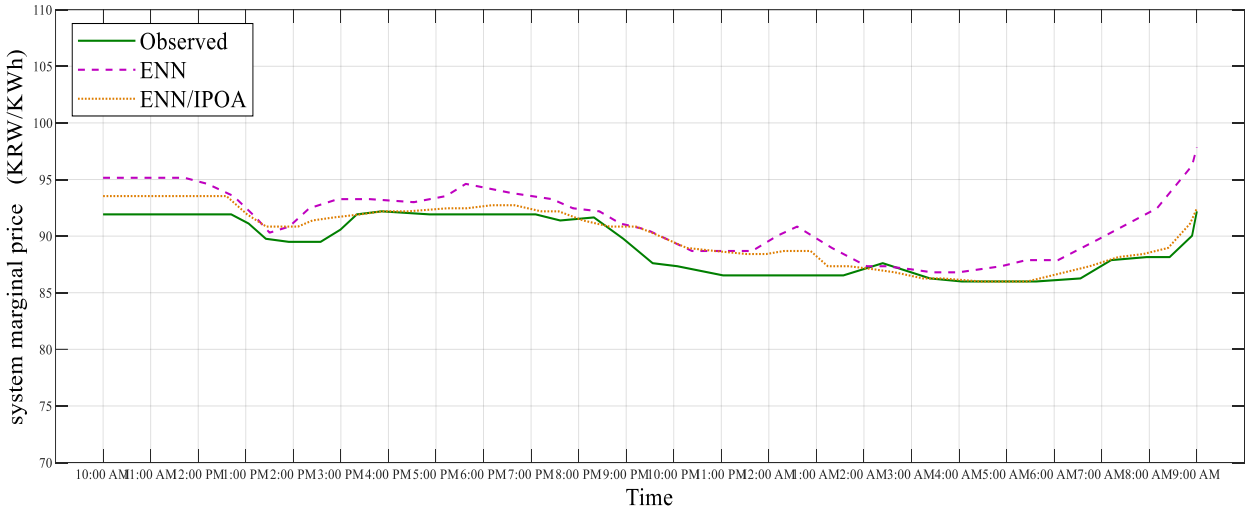

Fig. 9: Outcomes of the System Marginal Price Prediction for January 19

7. Conclusion

Electric energy plays a vital role in enhancing national prosperity and driving economic development. It differs from other energy carriers due to its unique characteristics, namely the requirement for real-time balance between supply and demand and the impracticality of storing it in large quantities. Ensuring a reliable electricity supply remains a primary objective for sector managers, given the significant economic losses associated with service interruptions. Historically, the substantial investments required for electricity generation, transmission, and distribution justified the establishment of government monopolies in the industry. In such monopoly markets, electricity pricing is determined according to government social and industrial policies, taking into account energy costs, productivity, and the structure and type of production. In this study, a novel approach based on a modified ENN was proposed for day-ahead SMP forecasting using long-term historical data. An enhanced version of the POA was employed to optimise the modified ENN. The discrete Fréchet distance was applied to long-term input variables, which were further augmented with temporal covariates, including seasonal indicators (summer/winter) and categorical day-type classifiers (weekday/holiday). Fifteen years of predicted load and actual SMP data for Korea were utilised, and the outcomes were validated against a non-optimised model. The results demonstrated that the proposed approach outperforms traditional forecasting models in accurately predicting SMP.

References

[1] Aghajani, G., & Ghadimi, N. (2018). Multi-objective energy management in a micro-grid. *Energy Reports*, *4*, 218-225. https://doi.org/10.1016/j.egyr.2017.10.002

[2] Akbary, P., Ghiasi, M., Pourkheranjani, M. R. R., Alipour, H., & Ghadimi, N. (2019). Extracting appropriate nodal marginal prices for all types of committed reserve. *Computational Economics*, *53*(1), 1-26. https://doi.org/10.1007/s10614-017-9716-2

[3] Alferaidi, A., Yadav, K., Alharbi, Y., Razmjooy, N., Viriyasitavat, W., Gulati, K., Kautish, S., & Dhiman, G. (2022). Distributed Deep CNN-LSTM Model for Intrusion Detection Method in IoT-Based Vehicles. *Mathematical Problems in Engineering*, *2022*(1), 3424819. https://doi.org/10.1155/2022/3424819

[4] Anastasiadis, A., Konstantinopoulos, S., Kondylis, G., Vokas, G. A., & Salame, M. J. (2018). Carbon tax, system marginal price and environmental policies on Smart Microgrid operation. *Management of Environmental Quality: An International Journal*, *29*(1), 76-88. https://doi.org/10.1108/MEQ-11-2016-0086

[5] Bagheri, M., Nurmanova, V., Abedinia, O., Naderi, M. S., Naderi, M. S., & Ghadimi, N. (2018). A novel wind power forecasting based feature selection and hybrid forecast engine bundled with honey bee mating optimization. 2018 IEEE International Conference on Environment and Electrical Engineering and 2018 IEEE Industrial and Commercial Power Systems Europe (EEEIC/I&CPS Europe), 1-6. https://doi.org/10.1109/EEEIC.2018.8493805

[6] Bahmanyar, D., Razmjooy, N., & Mirjalili, S. (2022). Multi-objective scheduling of IoT-enabled smart homes for energy management based on Arithmetic Optimization Algorithm: A Node-RED and NodeMCU module-based technique. *Knowledge-Based Systems*, *247*, 108762. https://doi.org/10.1016/j.knosys.2022.108762

[7] Cai, W., Mohammaditab, R., Fathi, G., Wakil, K., Ebadi, A. G., & Ghadimi, N. (2019). Optimal bidding and offering strategies of compressed air energy storage: A hybrid robust-stochastic approach. *Renewable Energy*, *143*, 1-8. https://doi.org/10.1016/j.renene.2019.05.008

[8] Cao, Y., Li, Y., Zhang, G., Jermsittiparsert, K., & Razmjooy, N. (2019). Experimental modeling of PEM fuel cells using a new improved seagull optimization algorithm. *Energy Reports*, *5*, 1616-1625. https://doi.org/10.1016/j.egyr.2019.11.013

[9] Cao, Y., Wu, Y., Fu, L., Jermsittiparsert, K., & Razmjooy, N. (2019). Multi-objective optimization of a PEMFC based CCHP system by meta-heuristics. *Energy Reports*, *5*, 1551-1559. https://doi.org/10.1016/j.egyr.2019.10.029

[10] Dehghani, M., Ghiasi, M., Niknam, T., Kavousi-Fard, A., Shasadeghi, M., Ghadimi, N., & Taghizadeh-Hesary, F. (2020). Blockchain-based securing of data exchange in a power transmission system considering congestion management and social welfare. *Sustainability*, *13*(1), 90. https://doi.org/10.3390/su13010090

[11] Ebrahimian, H., Barmayoon, S., Mohammadi, M., & Ghadimi, N. (2018). The price prediction for the energy market based on a new method. *Economic research-Ekonomska istraživanja*, *31*(1), 313-337. https://doi.org/10.1080/1331677X.2018.1429291

[12] Eiter, T., & Mannila, H. (1994). Computing discrete Fréchet distance. https://www.kr.tuwien.ac.at/staff/eiter/et-archive/files/cdtr9464.pdf

[13] Eslami, M., Moghadam, H. A., Zayandehroodi, H., & Ghadimi, N. (2019). A new formulation to reduce the number of variables and constraints to expedite SCUC in bulky power systems. *Proceedings of the national academy of sciences, india section a: physical sciences*, *89*(2), 311-321. https://doi.org/10.1007/s40010-017-0475-1

[14] Fan, X., Sun, H., Yuan, Z., Li, Z., Shi, R., & Ghadimi, N. (2020). High voltage gain DC/DC converter using coupled inductor and VM techniques. *IEEE Access*, *8*, 131975-131987. https://doi.org/10.1109/ACCESS.2020.3002902

[15] Fan, X., Sun, H., Yuan, Z., Li, Z., Shi, R., & Razmjooy, N. (2020). Multi-objective optimization for the proper selection of the best heat pump technology in a fuel cell-heat pump micro-CHP system. *Energy Reports*, *6*, 325-335. https://doi.org/10.1016/j.egyr.2020.01.009

[16] Fei, X., Xuejun, R., & Razmjooy, N. (2023). Optimal configuration and energy management for combined solar chimney, solid oxide electrolysis, and fuel cell: a case study in Iran. *Energy sources, Part A: recovery, utilization, and environmental effects*, *45*(4), 9794-9814. https://doi.org/10.1080/15567036.2019.1680770

[17] Firouz, M. H., & Ghadimi, N. (2016). Concordant controllers based on FACTS and FPSS for solving wide-area in multi-machine power system. *Journal of Intelligent & Fuzzy Systems*,

30(2), 845-859. https://doi.org/10.3233/IFS-151807

[18] Gao, W., Darvishan, A., Toghani, M., Mohammadi, M., Abedinia, O., & Ghadimi, N. (2019). Different states of multi-block based forecast engine for price and load prediction. *International Journal of Electrical Power & Energy Systems*, *104*, 423-435. https://doi.org/10.1016/j.ijepes.2018.07.014

[19] Gong, W., & razmjooy, N. (2022). A new optimisation algorithm based on OCM and PCM solution through energy reserve. *International Journal of Ambient Energy*, *43*(1), 2299-2312. https://doi.org/10.1080/01430750.2020.1730952

[20] Guo, Y., Dai, X., Jermsittiparsert, K., & Razmjooy, N. (2020). An optimal configuration for a battery and PEM fuel cell-based hybrid energy system using developed Krill herd optimization algorithm for locomotive application. *Energy Reports*, *6*, 885-894. https://doi.org/10.1016/j.egyr.2020.04.012

[21] Jain, M., Maurya, S., Rani, A., & Singh, V. (2018). Owl search algorithm: a novel nature-inspired heuristic paradigm for global optimization. *Journal of Intelligent & Fuzzy Systems*, *34*(3), 1573-1582. https://doi.org/10.3233/JIFS-169452

[22] Leng, H., Li, X., Zhu, J., Tang, H., Zhang, Z., & Ghadimi, N. (2018). A new wind power prediction method based on ridgelet transforms, hybrid feature selection and closed-loop forecasting. *Advanced Engineering Informatics*, *36*, 20-30. https://doi.org/10.1016/j.aei.2018.02.006

[23] Li, X., Niu, P., & Liu, J. (2018). Combustion optimization of a boiler based on the chaos and Levy flight vortex search algorithm. *Applied Mathematical Modelling*, *58*, 3-18. https://doi.org/10.1016/j.apm.2018.01.043

[24] Liu, J., Chen, C., Liu, Z., Jermsittiparsert, K., & Ghadimi, N. (2020). An IGDT-based risk-involved optimal bidding strategy for hydrogen storage-based intelligent parking lot of electric vehicles. *Journal of Energy Storage*, *27*, 101057. https://doi.org/10.1016/j.est.2019.101057

[25] Mir, M., Shafieezadeh, M., Heidari, M. A., & Ghadimi, N. (2020). Application of hybrid forecast engine based intelligent algorithm and feature selection for wind signal prediction. *Evolving Systems*, *11*(4), 559-573. https://doi.org/10.1007/s12530-019-09271-y

[26] Mirjalili, S., Mirjalili, S. M., & Hatamlou, A. (2016). Multi-verse optimizer: a nature-inspired algorithm for global optimization. *Neural computing and applications*, *27*(2), 495-513. https://doi.org/10.1007/s00521-015-1870-7

[27] Mirzapour, F., Lakzaei, M., Varamini, G., Teimourian, M., & Ghadimi, N. (2019). A new prediction model of battery and wind-solar output in hybrid power system. *Journal of Ambient Intelligence and Humanized Computing*, *10*(1), 77-87. https://doi.org/10.1007/s12652-017-0600-7

[28] Noh, J., & Cho, H. C. (2020). Forecasting System Marginal Price Using Multilayer Perceptron and Nonlinear Autoregressive exogenous model. *Journal of the Korean Society of Mineral and Energy Resources Engineers*, *57*(6), 585-592. https://doi.org/10.32390/ksmer.2020.57.6.585

[29] Ramezani, M., Bahmanyar, D., & Razmjooy, N. (2021). A new improved model of marine predator algorithm for optimization problems. *Arabian Journal for Science and Engineering*, *46*(9), 8803-8826. https://doi.org/10.1007/s13369-021-05688-3

[30] Rim, C., Piao, S., Li, G., & Pak, U. (2018). A niching chaos optimization algorithm for multimodal optimization. *Soft Computing*, *22*(2), 621-633. https://doi.org/10.1007/s00500-016-2360-2

[31] Shin, S., & Yoo, H. (2021). An Error Correction Model for Long Term Forecast of System

Marginal Price. *Journal of the Korea Academia-Industrial cooperation Society*, *22*(6), 453-459.

[32] Sun, L., Han, X.-F., Xu, Y.-P., & Razmjooy, N. (2021). Exergy analysis of a fuel cell power system and optimizing it with Fractional-order Coyote Optimization Algorithm. *Energy Reports*, *7*, 7424-7433. https://doi.org/10.1016/j.egyr.2021.10.098

[33] Tian, M.-W., Yan, S.-R., Han, S.-Z., Nojavan, S., Jermsittiparsert, K., & Razmjooy, N. (2020). New optimal design for a hybrid solar chimney, solid oxide electrolysis and fuel cell based on improved deer hunting optimization algorithm. *Journal of Cleaner Production*, *249*, 119414. https://doi.org/10.1016/j.jclepro.2019.119414

[34] Yang, Z., Ghadamyari, M., Khorramdel, H., Alizadeh, S. M. S., Pirouzi, S., Milani, M., Banihashemi, F., & Ghadimi, N. (2021). Robust multi-objective optimal design of islanded hybrid system with renewable and diesel sources/stationary and mobile energy storage systems. *Renewable and Sustainable Energy Reviews*, *148*, 111295. https://doi.org/10.1016/j.rser.2021.111295

[35] Yang, Z., Liu, Q., Zhang, L., Dai, J., & Razmjooy, N. (2020). Model parameter estimation of the PEMFCs using improved barnacles mating optimization algorithm. *Energy*, *212*, 118738. https://doi.org/10.1016/j.energy.2020.118738

[36] Ye, H., Jin, G., Fei, W., & Ghadimi, N. (2024). High step-up interleaved dc/dc converter with high efficiency. *Energy sources, Part A: recovery, utilization, and environmental effects*, *46*(1), 4886-4905. https://doi.org/10.1080/15567036.2020.1716111

[37] Yu, D., Wang, Y., Liu, H., Jermsittiparsert, K., & Razmjooy, N. (2019). System identification of PEM fuel cells using an improved Elman neural network and a new hybrid optimization algorithm. *Energy Reports*, *5*, 1365-1374. https://doi.org/10.1016/j.egyr.2019.09.039

[38] Yuan, Z., Wang, W., Wang, H., & Razmjooy, N. (2020). A new technique for optimal estimation of the circuit-based PEMFCs using developed sunflower optimization algorithm. *Energy Reports*, *6*, 662-671. https://doi.org/10.1016/j.egyr.2020.03.010

[39] Zhi, Y., Weiqing, W., Haiyun, W., & Razmjooy, N. (2021). New approaches for regulation of solid oxide fuel cell using dynamic condition approximation and STATCOM. *International Transactions on Electrical Energy Systems*, *31*(2), e12756. https://doi.org/10.1002/2050-7038.12756

[40] Δαρδαμάνης, Α. (2022). *Evaluation of machine learning models for predicting the system marginal price of an electricity system–Italian SMP Day-Ahead forecasting* Πανεπιστήμιο Πειραιώς]. http://dx.doi.org/10.26267/unipi_dione/1944